Electrodeposition of platinum nanoparticles on polypyrrole-functionalized graphene

Wengao Zhao · Xibin Zhou · Zhonghua Xue · Bowan Wu · Xiuhui Liu · Xiaoquan Lu

Abstract In this study, the new electrocatalyst of platinum support on polypyrrole-functionalized graphene (GNS–PPy/PtNPs) is reported. The polypyrrole-functionalized graphene (GNS–PPy) is constructed first with graphene nanosheets (GNS) and polypyrrole (PPy) particles by constant potential deposition. And then PtNPs are deposited on the surface of GNS–PPy by cyclic voltammetry. The as-prepared GNS–PPy/PtNPs is characterized by scanning electron microscopy, energy-dispersive spectroscopy, X-ray powder diffraction, X-ray photoelectron spectroscopy, and Raman spectroscopy. The prepared GNS–PPy/PtNPs catalyst is employed for methanol oxidation reactions. Compared with GNS/PtNPs and PPy/PtNPs, the GNS–PPy/PtNPs has higher catalytic activity (508 mA/mg), better stability, and stronger poisoning-tolerance ($I_f/I_b = 4.18$) due to high dispersion of PtNPs on large surface of GNS–PPy as well as synergic effect among the GNS, PPy particles, and PtNPs. The experimental results indicate that GNS–PPy/PtNPs may be an ideal candidate catalyst for direct methanol fuel cell.

Introduction

Recently, fuel cells have received increasing attention due to the depletion of fossil fuels and increasingly severe environmental pollution. Among different types of fuel cells, direct methanol fuel cell (DMFC) is an excellent power source because of its high energy density, low pollution emission, low operating temperature, and ease of handing liquid fuel. However, there are still some critical obstacles inhibiting broad application of DMFC, including high cost of noble metal platinum (Pt)-based catalysts and the poisoning of the anode catalyst by adsorbed carbonyl species formed in the methanol oxidation process [1]. The catalyst tolerance to carbonaceous species accumulation can be described by the ratio of the forward anodic peak current I_f to the reverse anodic peak current I_b [2, 3]. High ratio of I_f/I_b indicates that methanol is efficiently oxidized to CO_2 and less accumulation of carbonaceous residues on the surface of catalyst [4–7]. In order to enhance the poisoning-tolerance and reduce the usage of Pt-based catalyst, it is necessary to seek suitable supports for effective dispersion of catalyst particles [8].

It is well known that graphene has high conductivity, large specific surface area (2630 m^2/g), and good stability [9], which is employed as an ideal platform for growing or anchoring metal functional nanomaterials [10, 11]. Several publications have been reported the application of graphene as substrate material for dispersion of Pt particles in DMFCs [12–16]. Usually, the two effective ways are used to prepare graphene/PtNPs. One strategy is to obtain PtNPs by chemical reduction. For instance, Choi [12] prepared the graphene/Pt composite with high platinum loading (1 mg/ml), which exhibited low mass activity (300 mA/mg) and I_f/I_b (<1). In addition, Wang and co-workers [17] synthesized the PVP–graphene/PtPd. Although the mass activity (647 mA/mg) is very high, the value of I_f/I_b is only 1.25. The other is to prepare PtNPs composites by electrodeposition. For example, Xia [14] synthesized the PtNPs@graphene by the method of amperometric I–t curve, which has low mass activity (195 mA/mg) and I_f/I_b value (1.26). Cai and co-workers [18] employed constant potential

W. Zhao · X. Zhou · Z. Xue · B. Wu · X. Liu · X. Lu (✉)
Key Laboratory of Bioelectrochemistry & Environment Analysis of Gansu Province, College of Chemistry & Chemical Engineering, Northwest Normal University, Lanzhou 730070, People's Republic of China
e-mail: taaluxq@126.com

Ⓐ Springer

electrodeposition to prepare PtAu/graphene catalysts. The mass activity is high (394 mA/mg), but the value of I_f/I_b is only 1.25. Therefore, seeking for the effective strategies to synthesize strong poisoning-tolerance and well-dispersed graphene-based catalyst is still a major topic of interest.

PPy with highly accessible surface area and high stability has been used to improve the activity of carbon support and enhance the dispersing of metal [19–21]. PPy-functionalized graphene and PPy-functionalized graphene oxide were extensively employed for supercapacitor due to its high electronic conductivity and easier charge transfer [22–26]. Moreover, PPy covered on the surface of graphene was used as a highly efficient and low-cost electrically switched ion exchanger for removing ClO_4^- from wastewater [27]. More encouragingly, an excellent report has also been seen using Pd/polypyrrole–graphene as the catalyst in methanol solution [28]. However, to the best of our knowledge, so far there have been no reports about the new catalysts of Pt supported on PPy/graphene composites for DMFC application. So, in our work, we investigated the property of GNS–PPy/PtNPs for methanol oxidation reactions (MORs), which exhibits strong poisoning-tolerance and high catalytic activity because of high electronic conductivity, easier charge transfer, and rough surface of GNS–PPy. Furthermore, the content of Pt metal in the catalyst is remarkably reduced, resulting in low cost of prepared catalyst.

Experiment

Materials

Graphene was purchased from Beijing Jiansin technological company (China) and was prepared by arc discharge method. Pyrrole was purchased from Beijing leadership chemical company (China), which was double distilled and then was kept in a refrigerator before use. $H_2PtCl_6 \cdot 6H_2O$ and CH_3OH were obtained from Beijing chemical company, China. All chemicals were of analytical-reagent grade and were used without further purification.

Apparatus

All electrochemical measurements were carried out by CHI 660C electrochemical workstation (CH instruments). A three-electrode configuration (glassy carbon work electrode (GCE), Ag/AgCl reference electrode, and platinum wire counter electrode) was used in all experiments. The surface morphology of the GNS–PPy/PtNPs was observed by field emission scanning electron microscopy (FE-SEM, Hitachi S-4800). All samples were sputtered gold before scanning by SEM.

The structure of GNS–PPy was examined by Raman spectroscopy (Renishaw invia, $\lambda = 633$ nm). The obtained catalyst was analyzed by X-ray diffraction (D/Max-2400, $\lambda = 0.1542$ nm) to determine the film structures. The catalyst compositional information was obtained with an energy-dispersive spectrometer (EDS) analyzer associated with FE-SEM (Hitachi S-4800). XPS (Phi5702) measurement was performed on spectrometer with Al Kα X-ray radiation as the X-ray source for excitation. Pt loadings on the modified electrodes were measured on an IRISER/S inductively coupled plasma spectrum instrument (ICP) (TJA, America). A conductive copper wire connected to a slice of glassy carbon (the diameter is 5 mm), and then which was sealed by nonconductive adhesive tape as a work electrode, the catalyst were electrodeposited on the surface of the slice of glassy carbon, and which was used as the sample for all test, such as SEM, XRD, and ICP, etc.

Preparation of the GNS–PPy/PtNPs-modified GCE

GCE was polished with 0.3, 0.05 μm alumina powders, followed by sonication with acetone, ethanol, and water, respectively. 2 mg GNS was suspended into 2 ml dimethylformamide and dispersed for 30 min. GNS suspension was casted on the surface of GCE and dried with an infrared lamp. Electropolymerization of pyrrole on the GNS-modified GCE was carried out in the solution containing 0.05 M pyrrole with 0.1 M $LiClO_4$ and 0.1 M $NaHCO_3$ at a constant potential of 0.8 V for 20 s [29, 30].

The GNS–PPy-modified GCE was further treated by cyclic voltammetry (CV) from 0.40 to −0.20 V in 0.5 M H_2SO_4 + 2.0 mM H_2PtCl_6 at a scan rate of 50 mV/s for depositing PtNPs on the rough surface of GNS–PPy. When electrodeposition cycle numbers was few, the catalytical activity is low, and while cycle number was more than 40, the catalytical activity is weak because of PtNPs aggregation. So the cycle numbers was chosen as 40, and the loading mass (29.28 μg/cm^2) of PtNPs was measured by ICP. For comparison, the same numbers of scanning cycle (40) were employed on GNS and PPy, which were denoted as GNS/PtNPs and PPy/PtNPs for MORs.

Schematic diagram of prepared GNS–PPy/PtNPs

The whole procedure for preparing the GNS–PPy/PtNPs was shown in Scheme 1. First, 2.5 μl GNS suspension (1 mg/ml) was casted on the surface of GCE. Second, irregular shape of the PPy particles were deposited on the surface of GNS by amperometric I–t curves. Finally, $PtCl_6^{2-}$ was absorbed on GNS–PPy surface, and PtNPs were deposited on the surface of GNS–PPy by CV.
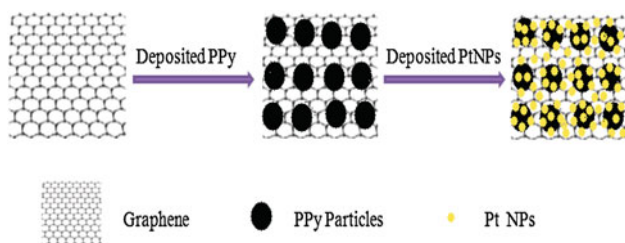
Scheme 1 Schematic diagram of prepared GNS–PPy/PtNPs. (a) GNS suspension was dispersed on glass carbon electrode surface, (b) the irregular shape of the PPy particles were deposited on the surface of GNS, (c) PtNPs were deposited on the surface of GNS–PPy

Results and discussion

Characterization of the microstructure of GNS–PPy/PtNPs

SEM

Figure 1 shows the SEM images of the GNS, GNS–PPy, and GNS–PPy/PtNPs, respectively. As shown in Fig. 1a, sheet-like graphene (200–500 nm) with crimple can be observed. Graphene, excellent carbon material with large surface area, superior chemical stability, and low production cost, could act as an ideal substrate for depositing functional materials for high-performance electrocatalytic or electrochemical devices [20–25, 27]. In addition, higher crystallinity and electroactivity of graphene was prepared by arc discharge method in our experiment, which can improve the mobility of charge carriers and stability [31, 32]. Figure 1b represents the rough surface of the GNS–PPy. GNS was functionalized by irregular PPy particles with the size of 400–800 nm. The PPy particles are loose and contains many spherical particles forming a three-dimensional (3D) porous nanostructure which can be highly beneficial for ion diffusion [30]. Figure 1c shows the surface morphology of GNS–PPy/PtNPs. The PtNPs (ca. 50 nm) were dispersed uniformly on the surface of the PPy–graphene without obvious agglomeration. The oxidized PPy conducting polymeric chain contains positive charge, and the charge must be balanced by the dopant counter ion. In addition, the 3D porous nanostructure of the GNS–PPy facilitates $PtCl_6^{2-}$ to easily diffuse into surface of the composite film. The embedded Pt nanoclusters were generated by a solid-phase extraction of $PtCl_6^{2-}$ species by the PPy, which then could be further reduced to the Pt(0) state and congregated into 3D structures [33, 34].

EDS, XPS, and XRD

EDS analysis was utilized to determine the composition of the GNS–PPy/PtNPs catalyst. In Fig. 2a, the carbon, nitrogen, and oxygen signals indicate that PPy is completely
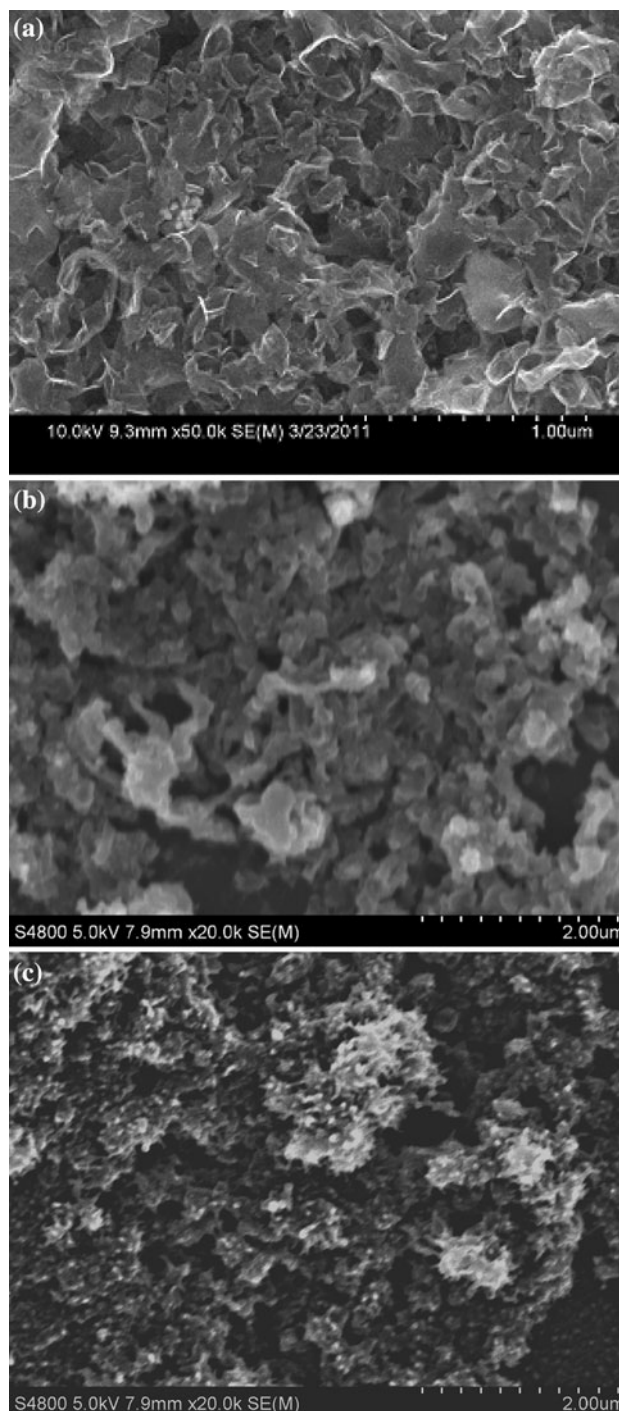

Fig. 1 SEM images of catalysts. **a** GNS, **b** GNS–PPy, **c** GNS–PPy/PtNPs

composited with GNS, and platinum signal results from PtNPs by electrodeposition. Similar results are observed for GNS/PtNPs and PPy/PtNPs. The formation of GNS–PPy/PtNPs is further characterized by XPS. In Fig. 2b–d, XPS patterns show significant C (Fig. 2b) signal corresponding to the binding energy of C_{1s} (from polypyrrole), and the C1s shoulder peaks at around 283.5 eV to the graphene

decorated Pt crystallinity surface [33, 34]. N signal (Fig. 2c) corresponding to the binding energy of N (from polypyrrole), significant Pt4f signals (Fig. 2d), the two bands appear at 71.4 and 74.8 eV, corresponding to the $Pt4f_{7/2}$ and $Pt4f_{5/2}$ signals, respectively. The result shows that the precursor of $H_2PtCl_6 \cdot 6H_2O$ is converted completely into Pt(0) under the experimental conditions. XRD patterns of GNS–PPy/PtNPs,

GNS/PtNPs, and PPy/PtNPs catalysts are shown in Fig. 2e. The peaks at $2\theta = 26.3$ is associated with the C (002) planes of the graphene or PPy [35, 36]. The (111), (200), (220), and (311) planes display a typical diffraction pattern of face-centered cubic (fcc) lattice for PtNPs [37, 38]. The result is accordant with EDS and XPS, indicating PtNPs were deposited on the surface of GNS–PPy.
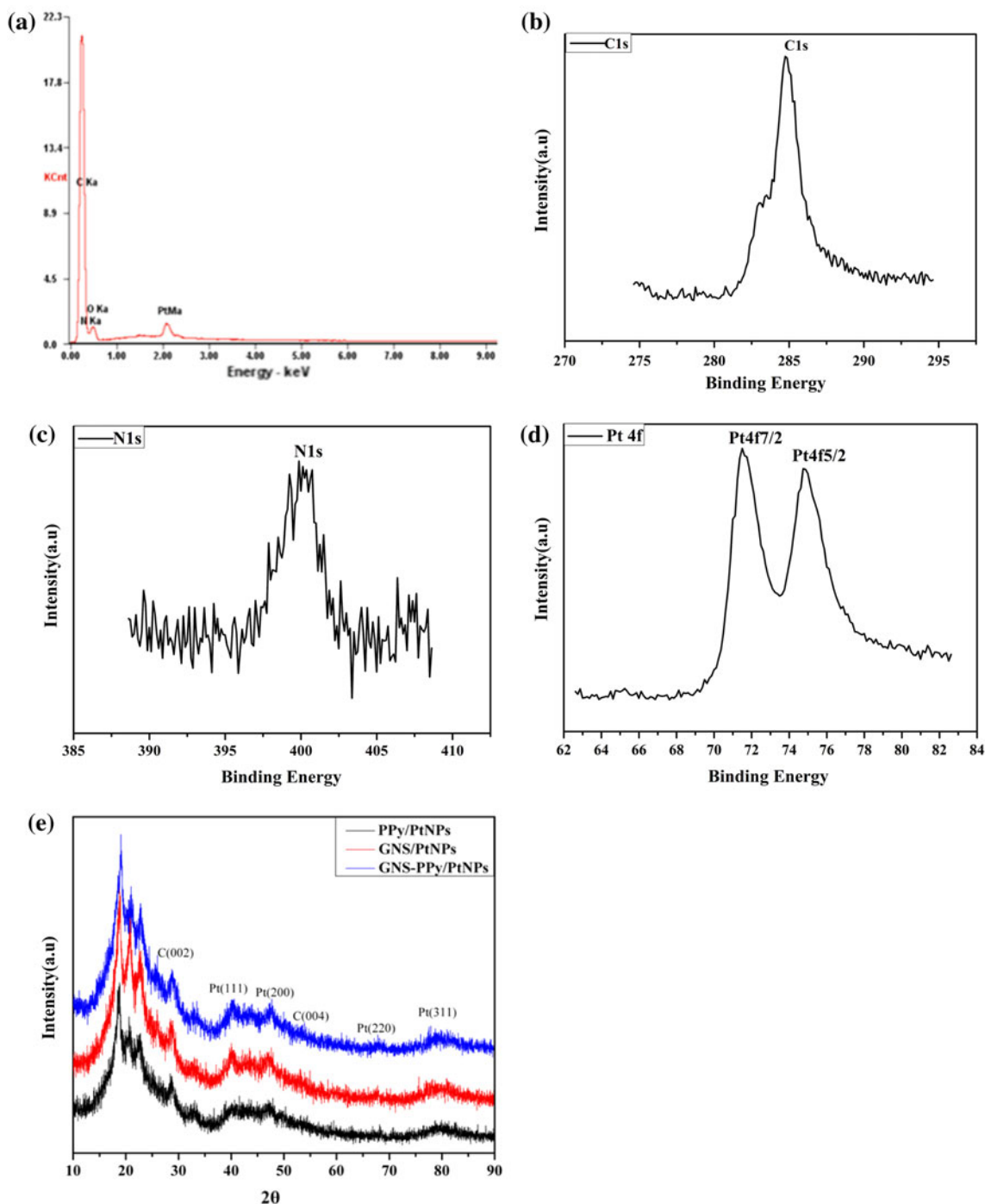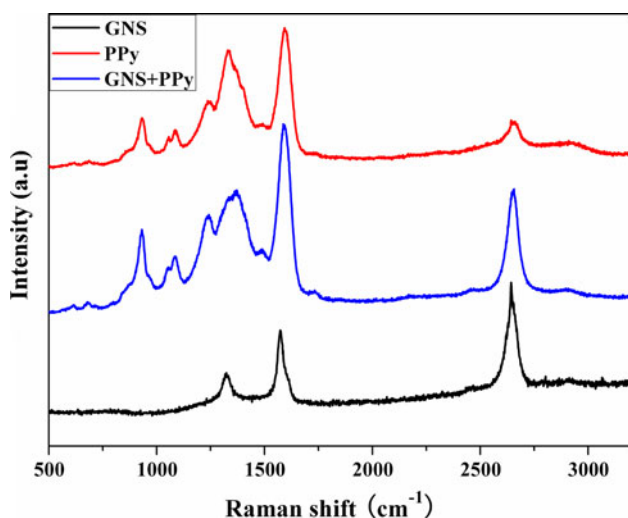

Fig. 2 The microstructure of GNS–PPy/PtNPs was characterized by EDS, XPS and XRD patterns. (**a**) EDS image; (**b–d**) XPS images of the catalyst, (**b**) C, (**c**) N, (**d**) Pt; (**e**) XRD pattern

Raman spectroscopy

Raman spectroscopy is one of the useful tools for providing detailed structure information [39]. The interaction between the PPy particles and the aromatic graphene basal plane is investigated by Raman spectra. In Fig. 3, for GNS sample, the high intensity of the G band peak at 1582 cm^{-1} as compared to the low intensity "disordered and defect" D band peak at 1321 cm^{-1} demonstrates the aromatic purity of the graphene basal plane [40]. The 2D (2660 cm^{-1}) band in single layer graphene (SLG) can be fit to a single Lorentzian peak and its intensity has been found to be much higher than that of the G band (located at ∼1580 cm^{-1}) for SLG; hence, it is often used as an indicator of a SLG region [41–45]. For the PPy nanoparticles sample, the appearance of peaks near 1598 and 1355 cm^{-1} arises from the π-conjugated structure and ring stretching mode of the polymer backbone, respectively [46–49]. The broad peak obtained at 1056 cm^{-1} corresponds to the C–H in-plane deformation. Two small peaks near 935 cm^{-1} are associated with the quinoid polaronic structure. In addition, because LiClO$_4$ and NaHCO$_3$ are doped at the process of electrodeposition PPy, C–OH stretching at 1246 cm^{-1}, C–O vibration at 1079 cm^{-1}, the peak observed at 868 cm^{-1} might be assigned to the =C–H out of plane vibration. With the depositing of PPy particles on the GNS, the Raman spectrum is essentially composed of both PPy particles and GNS. For thin film of composites, the appearance of bands near 1056, 935, 1246, 1079, and 868 cm^{-1} are identical to the single PPy particles. However, as compared with the single PPy sample, the decrease in the ratio of the sharp G band peak at 1586.1 cm^{-1} as compared to the defect band near 1285.4 cm^{-1} reflects the interaction between the π-conjugated particles and

aromatic graphene basal plane without compromising the chemical identity of either of these two nanomaterials. In addition, the GNS–PPy shows no increase in the 2D peak (the graphene 2D peak) compared to GNS, which indicate that PPy do not destroy the structure of SLG.

Electrochemical surface areas of the catalysts

In Fig. 4, the electrochemical active surface areas (EAS, m^2/g) of the catalysts can be measured by integrating Coulombic charge for hydrogen adsorption (Q_H) on the CV curves in N$_2$-purged 0.5 M H$_2$SO$_4$ solution [50]. The region for hydrogen adsorption (−0.2 to 0 V vs. Ag/AgCl electrode) is used to estimate the EAS according to the following equation [51]:

$$EAS = \frac{Q_H}{0.21 \times L_{Pt}},$$

where the L_{Pt} is the Pt loading mass (mg), Q_H is the charge for H$_2$ adsorption, and 0.21 is the charge required to oxidize a monolayer of H$_2$ on smooth Pt (mC cm^{-2}). A_r (cm^2) is the PtNPs real surface area, which can be estimated from $A_r = Q_H/0.21$. The roughness factor (ρ) can be obtained from the ratio of A_r and geometric area (A_g) of the electrode. The loading mass of PtNPs is estimated by ICP. The ρ, EAS (m^2/g), and mass activities (mA/mg) of MORs at GNS–PPy/PtNPs, GNS/PtNPs, and PPy/PtNPs are listed in Table 1. The GNS–PPy/PtNPs shows much higher EAS, larger ρ, and stronger mass activity compared to GNS/PtNPs and PPy/PtNPs. This may be attributed to the rougher surface and 3D structures of GNS–PPy/PtNPs. The particular structure significantly enhances EAS and ρ of the catalyst.


Fig. 3 Raman spectra image of GNS, PPy, and GNS–PPy
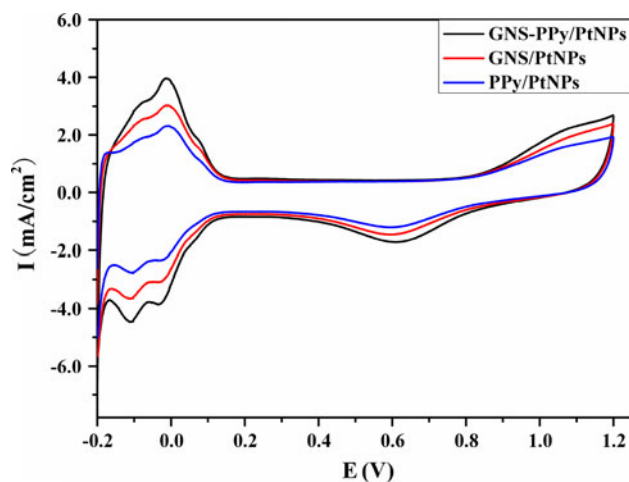
Fig. 4 Cyclic voltammograms of PPy/PtNPs, GNS/PtNPs, and GNS–PPy/PtNPs-modified GCE in a N$_2$-sparged 0.5 M H$_2$SO$_4$ solution at the scan rate of 50 mV/s

Table 1 Electrochemical characterization of GNS–PPy/PtNPs, GNS/PtNPs, and PPy/PtNPs

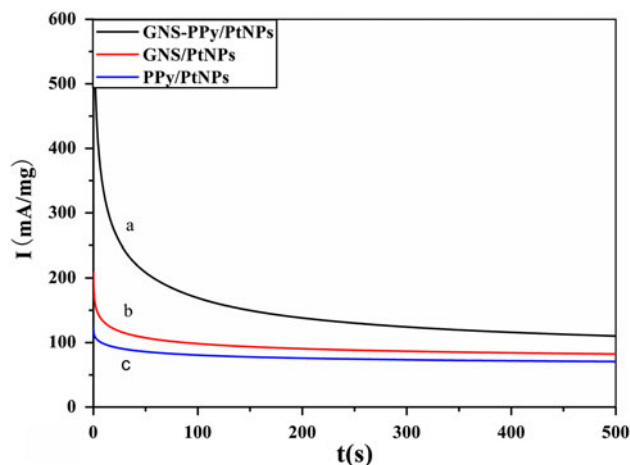|	PPy/PtNPs	GNS/PtNPs	GNS–PPy/PtNPs
Mass activity (mA/mg)	205	423	508
EAS (m^2/g)	31.38	40.71	50.2
Roughness factor (ρ)	8.6	13.9	21.8
Oxidatin potential (V)	0.769	0.784	0.754
I_f/I_b	1.43	3.36	4.18

Evaluation of methanol electro-oxidation

The catalytic activity for the prepared GNS–PPy/PtNPs, GNS/PtNPs, and PPy/PtNPs on the MORs was studied by CV recorded in 1.0 M H_2SO_4 containing 1.0 M methanol at a scan rate of 50 mV/s. Figure 5 represents the comparison of the mass activity on the different modified electrodes. The GNS–PPy/PtNPs has higher mass activity for MORs as compared with GNS/PtNPs and PPy/PtNPs. It should be noted that the mass activity of GNS–PPy/PtNPs is also higher than most Pt-based catalysts for MORs, such as carbon nanofibers or CNT-support PtNPs [37], CNT/Pt composite catalyst [52, 53], PPy/Pt composite catalyst [54], and GNS/PtNPs hybrids [55]. Meanwhile, GNS–PPy/PtNPs (0.30 V) has lower onset potential than GNS/PtNPs (0.38 V) and PPy/PtNPs (0.35 V). The onset potential relates to the breaking of C–H bonds and removal of the CO_{ads} like intermediates by oxidation with OH_{ads} species supplied by Pt–OH sites or other sources [56]. The lower onset potential of the methanol oxidation on GNS–PPy/PtNPs indicates that the oxidative removal of the
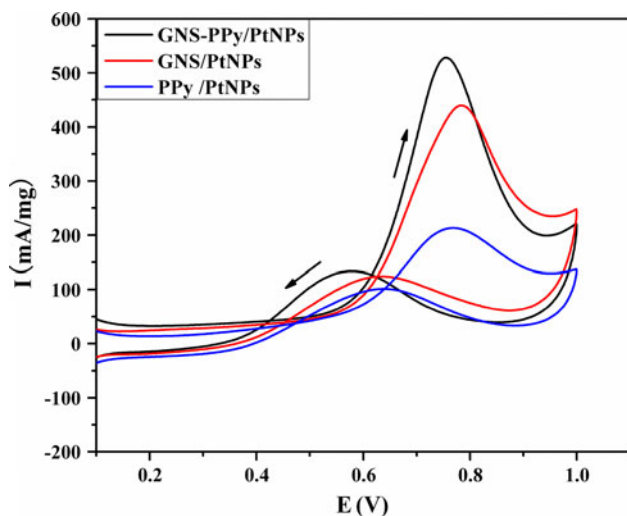
Fig. 5 Mass activity for methanol oxidation on the prepared GNS–PPy/PtNPs, GNS/PtNPs, and PPy/PtNPs catalysts; experiments were carried out in 0.5 M H_2SO_4 + 1.0 M CH_3OH at a scan rate of 50 mV/s. The *arrows* indicate the direction of potential sweep

Fig. 6 The amperometric *I–t* curves of catalysts. (*a*) GNS–PPy/PtNPs, (*b*) GNS/PtNPs, (*c*) PPy/PtNPs-modified GCE in a N_2-sparged 0.5 M H_2SO_4 solution containing 1.0 M methanol

intermediates generated from the methanol oxidation can occur easily as compared to GNS/PtNPs and PPy/PtNPs. The high ratio of the forward anodic peak current density (I_f) to the reverse anodic peak current density (I_b) indicates that the intermediate carbonaceous species are effectively oxidized to CO_2 in the forward scanning. The ratio is 1.43 for PPy/PtNPs, 3.36 for GNS/PtNPs, and 4.18 for the GNS–PPy/PtNPs. The results reveal that methanol is efficiently oxidized to CO_2 and a little accumulation of carbonaceous residues at the GNS–PPy/PtNPs surface [6, 7]. Moreover, the catalytic activity and poisoning-tolerance of GNS–PPy/PtNPs are better than most of catalysts, such as Pt nanorods [57], graphene oxide/Pt [58], and PtNi/C [59].

The long-term stability of the PPy/PtNPs, GNS/PtNPs, and GNS–PPy/PtNPs were examined using amperometric *I–t* curve. Figure 6 shows the tests recorded at a constant potential of 0.70 V in the solution containing 0.5 M H_2SO_4 + 1.0 M CH_3OH for 500 s. The current density decreased rapidly at the initial stage, gradually, the current decayed and a pseudo-steady state was achieved [60]. It was appeared that GNS–PPy/PtNPs maintained a better stability, and the mass activity was 110 mA/mg, which was higher than GNS/PtNPs (83 mA/mg) and PPy/PtNPs (68 mA/mg). Meanwhile, the performance is better than those of carbon nanotubes with Pt decorated on both the inner and the outer wall surfaces (about 92 % loss of current after 1000 s running) and Pt/CNT composites (about 77 % loss of current after 600 s running) [2, 61]. The oxidation current decreased continuously for all the catalysts due to the formation of a series of adsorbed carboxyl intermediates $(CH_xO)_{ads}$ ($x = 1–3$) and $(CO)_{ads}$, which gradually accumulated to lower the electroactive area of catalyst and significantly poisoned the PtNPs for the MORs [62, 63].

The efficiency of the catalysts in fuel cells is strongly related to the surface area and rough degree of the support materials as well as the dispersion and size of catalysts, which would improve the catalysts efficiency and decrease the loading mass level of precious metals used [63]. That is to say, higher mass activity, larger ESA, and stronger poisoning-tolerance in electrochemical performance were observed in the experiments can probably be attributed to two major factors: (i) GNS and PPy particles constructed 3D structures, which has rougher surface than GNS and PPy. The rough surface can prevent the aggregation of PtNPs, and make the PtNPs well dispersed on the surface of GNS–PPy; (ii) the composite of PPy–GNS has high electronic conductivity and easier charge transfer, which can increase the reaction rate of MOR. In addition, the synergic effects among GNS, PPy, and PtNPs can improve the catalytic activity and reduce the cost of catalyst.

Conclusions

In this paper, electrochemical methods have been employed to synthesize and characterize the GNS–PPy/PtNPs. The experimental results demonstrate that GNS–PPy/PtNPs is an attractive Pt-based catalyst for the MORs, which is attributed to the rough surface and large ECSAs. PtNPs are well dispersed on the surface of GNS–PPy, so the GNS–PPy/PtNPs exhibits higher catalytic activity and stability for MORs than GNS/PtNPs and PPy/PtNPs in acidity media. Moreover, GNS–PPy/PtNPs tolerance to carbonaceous species accumulation is superior to most of catalysts. These experimental results suggest that the GNS–PPy/PtNPs are a promising anode catalyst candidate for DMFC.

References

1. Dong LF, Gari RRS, Li Z, Michael MC, Hou SF (2010) Carbon 48:781
2. Lin YH, Cui XL, Ye C (2005) J Phys Chem B 109:14410
3. Liu ZL, Ling XY, Su XD, Lee JY (2004) J Phys Chem B 108:8234
4. Zhao M, Li J, Song Z, Desmond R, Tschaen DM, Grabowski EJJ, Reider PJ (1998) Tetrahedron Lett 39:5323
5. Keresszegi C, Ferri D, Mallat T, Baiker A (2005) J Phys Chem B 109:958
6. Abad A, Conception P, Corma A, Garcia H (2005) Angew Chem Int Ed 44:4066
7. Choudhary VR, Dumbre DK (2009) Ind Eng Chem Res 48:9471
8. Leela MRA, Ramaprabhu S (2007) J Phys Chem C 111:16138
9. Wang L, Tian CG, Wang H, Ma YG, Wang BL, Fu HG (2010) J Phys Chem C 114:8727
10. Yin HJ, Tang HJ, Wang D, Gao Y, Tang ZY (2012) ACS Nano 6:8288
11. Wang JF, Gao JX, Xiong YS, Yang JD, Gao Y, Lu XQ, Liu YL, Tang ZY (2011) Chem Commun 47:6894
12. Choi SM, Seo MH, Kim HJ, Kim WB (2011) Carbon 49:904
13. Li YM, Tang LH, Li JH (2009) Electrochem Commun 11:846
14. Zhou YG, Chen JJ, Wang FB, Sheng ZH, Xia XH (2010) Chem Commun 46:5951
15. Li YJ, Gao W, Ci LJ, Wang CM, Ajayan PM (2010) Carbon 48:1124
16. Brownson DAC, Kampouris DK, Banks CE (2011) J Power Sources 196:4873
17. Guo SJ, Dong SJ, Wang EK (2010) ACS Nano 4:547
18. Hu YJ, Zhang H, Wu P, Zhang H, Zhou B, Cai CX (2011) Phys Chem Chem Phys 13:4083
19. Zhao HB, Li L, Yang J, Zhang YM, Li H (2008) Electrochem Commun 10:876
20. Zhao HB, Li L, Yang J, Zhang YM (2008) J Power Sources 184:375
21. Zhao HB, Yang J, Li L, Li H, Wang JL, Zhang YM (2009) Int J Hydrogen Energy 34:3908
22. Zhang DC, Zhang X, Chen Y, Yu P, Wang CH, Ma YW, Zhang D (2011) J Power Sources 196:5990
23. Liu AR, Li C, Bai H, Shi GQ (2010) J Phys Chem C 114:22783
24. Zhang LL, Zhao SY, Tian XN, Zhao XS (2010) Langmuir 26:17624
25. Biswas S, Drzal LT (2010) Chem Mater 22:5667
26. Lu XJ, Dou H, Yuan CZ, Yang SD, Hao L, Zhang F, Shen LF, Zhang LJ, Zhang XG (2011) J Power Sources 197:319
27. Zhang S, Shao YY, Liu J, Aksay IA, Lin YH (2011) ACS Appl Mater Interfaces 3:3633
28. Zhao YC, Zhan L, Tian JN, Nie SL, Ning Z (2011) Electrochim Acta 56:1967
29. Diaz AF, Castillo JI (1980) J Chem Soc Chem Commun 397
30. Li J, Lin XQ (2007) J Electrochem Soc 154:1074
31. Edwards RS, Coleman KS (2012) Nanoscale. doi:10.1039/c0xx00000x
32. Subrahmanyam KS, Panchakarla LS, Govindaraj A, Rao CNR (2009) J Phys Chem C 113:4257–4259
33. Oshima C, Nagashima A (1997) J Phys 9:1
34. Imamura G, Saiki K (2011) J Phys Chem C 115:10000
35. Prabhuram J, Zhao TS, Tang ZK, Chen R, Liang ZX (2006) J Phys Chem B 110:5245
36. Guo G, Qin F, Yang D, Wang C, Xu H, Yang S (2008) Chem Mater 20:2291
37. Hsin YL, Hwang KC, Yeh CT (2007) J Am Chem Soc 129:9999
38. Guo JW, Zhao TS, Prabhuram CW, Chen WR (2005) Electrochim Acta 51:754
39. Urso LD, Compagnini G, Puglisi O, Scandurra A, Cataliotti RS (2007) J Phys Chem C 111:13547
40. Biswas S, Lawrence TD (2010) Chem Mater 22:5567
41. Ferrari AC, Meyer JC, Scardaci V, Casiraghi C, Lazzeri M, Mauri F, Piscanec S, Jiang D, Novoselov KS, Roth S, Geim AK (2006) Phys Rev Lett 97:187401
42. Rao R, Podila R, Suchikawa R, Katoch J, Tishler D, Rao AM, Ishigami M (2011) ACS Nano 5:1594
43. Gupta A, Chen G, Joshi P, Tadigadapa S, Eklund P (2006) Nano Lett 6:2667
44. Canc-ado L, Reina A, Kong J, Dresselhaus MG (2008) Phys Rev B 77:245408
45. Malard L, Pimenta M, Dresselhaus G, Dresselhaus M (2009) Phys Rep 473:51
46. Wu TM, Chang HL, Lin YW (2009) Compos Sci Technol 69:639

47. Fan J, Wan M, Zhu D, Chang B, Pan Z, Xie S (1999) J Appl Poly Sci 74:2605
48. Wanekaya AK, Lei Y, Bekyarova E, Chen W, Haddon R, Mulchandani A, Myung NV (2006) Electroanalysis 18:1047
49. Han G, Yuan J, Shi G, Wei F (2005) Thin Sol Films 474:64
50. Lai LF, Huang GM, Wang XF, Weng J (2011) Carbon 49:1581
51. Pozio A, Francesco MD, Cemmi A, Cardellini F, Giorgi L (2002) J Power Sources 105:13
52. Mu Y, Liang H, Hu J, Jiang L, Wan L (2005) J Phys Chem B 109:22212
53. Zheng SF, Hu JS, Zhong LS, Wan LJ, Song WG (2007) J Phys Chem C 111:11174
54. Ma YW, Jiang SJ, Jian GQ, Tao HS, Yu LS, Wang XB, Wang XZ, Zhu JM, Hu Z, Chen Y (2009) Energy Environ Sci 2:224
55. Li YM, Tang LH, Li JH (2009) Electrochem Commun 11:846
56. Wang SY, Jiang SP, White TJ, Guo J, Wang X (2009) J Phys Chem C 113:18935
57. He YB, Li GR, Wang ZL, Ou YN, Tong YX (2010) J Phys Chem C 114:19175
58. Sharma S, Ganguly A, Papakonstantinou P, Miao X, Li M, Hutchison J, Delichatsios M, Ukleja S (2010) J Phys Chem C 114:19459
59. Jiang Q, Jiang LH, Hou HY, Qi J, Wang SL, Sun GQ (2010) J Phys Chem C 114:19714
60. Jiang JH, Kucernak A (2003) J Electroanal Chem 543:187
61. Wen ZH, Wang Q, Li JH (2008) Adv Funct Mater 18:959
62. Zhang H, Yin YJ, Hu YJ, Li CY, Wu P, Wei SH, Cai CX (2010) J Phys Chem C 114:11861
63. Shang N, Papakonstantinou P, Wang P, Silva SRP (2010) J Phys Chem C114:15837